Seismic Analysis of Transmission Towers Considering Both Geometric and Material Nonlinearities

Ying-Hui Lei* and Yu-Lin Chien

Department of Civil Engineering, Tamkang University, Tamsui, Taiwan 251, R.O.C.

Abstract

In this paper, the dynamic behavior of a group of transmission towers linked together through electrical wires and subjected to a strong ground motion will be investigated in detail. In performing the seismic analysis, the wires and the towers concerned are modeled, respectively, by using the efficient cable elements and the 3-D beam elements considering both geometric and material nonlinearities. In addition, to enhance the practical usage of the analytical scheme, the strength capacities and the fracture occurrences for the main members of the transmission tower will be examined with the employment of the appropriate strength interaction equations. It is expected that by aid of this investigation, those who are engaged in code constitution or practical designing of transmission towers may gain a better insight into the roles played by the interaction force between towers and wires and by the configuration of the transmission towers under strong earthquake.

Key Words: Transmission Towers, Geometric and Material Nonlinearities

1. Introduction

The importance of the transmission tower on national economy and people's living has been well recognized. During the attack of the Ji-Ji earthquake, with a size of 7.3 in Ritcher magnitude, in Taiwan on Sept. 21, 1999, over two thousand four hundred residents were killed. Besides, the strong vibration of the ground motion has caused the collapse of a main transmission tower located in the central region of the state. As a result, the government was forced to take measures of reducing electricity supply for more than six weeks. During this period, a great living inconvenience was brought to the people, and a huge commercial loss was incurred in the high-tech industry of the island.

To achieve the aim of supplying electricity everywhere in a country, many transmission towers are hence built in the rugged circumstances of climbing mountains or crossing rivers. Accordingly, the elevation at which some tower structures are located may differ from that associated with other transmission towers. Moreover, the marching route of the tower procession in such circumstances may exhibit in an extremely irregular manner. This variation on either the elevation or the orientation of the geometric configuration for a group of transmission towers would certainly affect the interaction force between electrical wires and tower structures.

The conventional seismic analysis of transmission towers is usually undertaken by taking each of towers as an isolated structure without taking the strong traction given by high-voltage electrical wires lining up in various directions in the air into account. Furthermore, many of structural engineers were used to simply ignore all wire mass or to take the wire mass as the lumped mass affiliated with the tower in seismic analysis. The results obtained from such analytical schemes would not be able to reflect effectively the actual forced conditions of the tower structure itself as well as the base foundation be-

*Corresponding author. E-mail: demanad@mail.tku.edu.tw

neath it.

To describe properly the deformed behavior of the structural joints connecting tower members together is probably one of the most complicated tasks in tower analyses. The complicacies are mainly due to (1) the flexibility of joints behaving nonlinearly from the very onset of loading [1], (2) the joint slippage resulting from the providence of erection tolerance in the course of producing the bolt holes throughout tower members [1–3] and (3) the flexural deformations of the primary leg member, introduced from the secondary diagonal members jointed with the leg member by using bolted connections [2,4]. Since the transmission tower is usually constructed by using the rolled steel angles which are eccentrically connected one another, nonlinear seismic analysis with respect to such a structure is widely known extremely difficult when the flexural deformations of the angle-section members are intended to be taken into account. In consequence, a proof-loading or full-scale testing combined with a linear elastic analysis in which the assumption of axially loaded conditions is applied to all the component members has formed an integral part of the tower design in practice [4]. To simplify the calculations involved, the effects due to joint flexibility and bolt slippage will be neglected and each component member of the transmission tower is assumed to have a square shape of cross section in this paper. It is expected that the adoption of these assumptions would not lessen much the value of the findings regarding the variation tendency of the internal forces acting on tower members under various configurations of a group of transmission towers.

Being slender and tall in appearance, the transmission tower is destined to be susceptible to the effect of geometric nonlinearity. On the other hand, the phenomenon of material nonlinearity is often observed on the primary leg members especially for those in the lowermost part of the tower subjected to a strong ground motion. Accordingly, a sophisticated seismic analysis considering both geometric and material nonlinearities will be performed in this research.

2. Modeling of Structural System

All seismic analyses in this paper are undertaken with respect to the structural system composed of various portions including electrical wires, tower structures and end-restraint springs, as indicated in Figure 1. The formulation involved in the modeling of each portion of the system will be described in the following.

2.1 Electrical Wires and End-restraint Springs

Being highly flexible and undergoing significant deformations, the electrical wire should therefore be analyzed by taking the effect of geometric nonlinearity into account. The cable element proposed by Jayaraman and Knudson and having been verified to be accurate and efficient in acquiring the stiffness matrix and elemental nodal-forces will be used for the modeling of electrical wires [5].

Consider a cable element in the local coordinate system composed of Y_L- and Z_L-axes, with its two ends being denoted by I and J respectively, as sketched in Figure 2. The Y_LZ_L-plane is defined as the vertical stretched

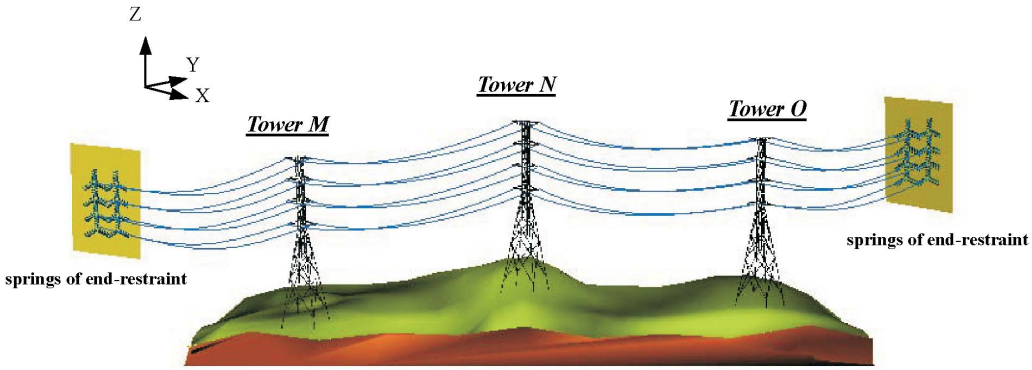

Figure 1. Analytical model of tower system.

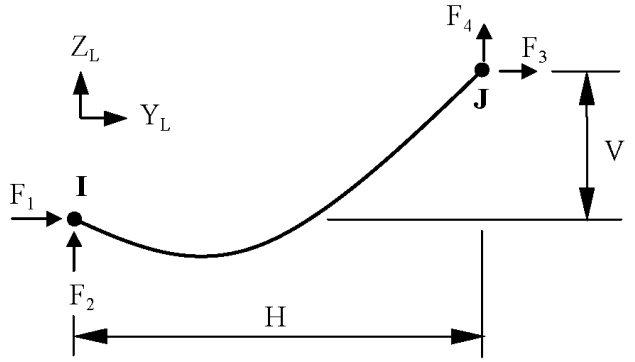

Figure 2. Cable element in local coordinate system.

plane containing the vector IJ and the force vector representing the self-weight of the element, and the positive direction of Y_L-axis is defined to be the same as that of Z-axis, namely the vertical axis of the global coordinate system. Letting F_1 and F_2 be the nodal-force components at end I in Y_L and Z_L directions respectively and F_3 and F_4 be those quantities at end J in Y_L and Z_L directions respectively, H and V be the distances between two ends measured along horizontal and vertical directions respectively, L_u and L be the unstressed and stressed lengths of the element respectively, T_I and T_J be the tensile forces acting at ends I and J respectively, w be the weight of the cable element per unit unstressed length, one can thus express the stressed shape of the cable element by using the following Eqs. [5–7]:

$$L = V^2 + H^2 \frac{\sinh^2 \lambda}{\lambda^2} \tag{1}$$

where

$$\lambda = \frac{w|H|}{2F_1} \tag{2}$$

$$F_2 = \frac{w}{2}\left[-V\frac{\cosh\lambda}{\sinh\lambda} + L\right] \tag{3}$$

$$H = -F_1\left[\frac{L_u}{EA} + \frac{1}{w}\log\frac{F_4 + T_J}{T_I - F_2}\right] \tag{4}$$

$$V = \frac{1}{2EAw}(T_J^2 - T_I^2) + \frac{T_J - T_I}{w} \tag{5}$$

$$L = L_u + \frac{1}{2EAw}\left[F_4T_J + F_2T_I + F_1^2\log\frac{F_4 + T_J}{T_I - F_2}\right] \tag{6}$$

The variables F_1, F_2, F_3, F_4, T_I and T_J are related by the following equations.

$$F_4 = -F_2 + wL_u \tag{7}$$
$$F_3 = -F_1 \tag{8}$$
$$T_I = (F_1^2 + F_2^2)^{1/2} \tag{9}$$
$$T_J = (F_3^2 + F_4^2)^{1/2} \tag{10}$$

It is observed from the above equations that H and V can be written in terms of F_1 and F_2 only. The infinitesimal variations in H and Vcan thus be approximated by their first order differentials as follows:

$$\delta H^i = \left(\frac{\partial H}{\partial F_1}\right)_i \delta F_1^i + \left(\frac{\partial H}{\partial F_2}\right)_i \delta F_2^i \tag{11}$$

$$\delta V^i = \left(\frac{\partial V}{\partial F_1}\right)_i \delta F_1^i + \left(\frac{\partial V}{\partial F_2}\right)_i \delta F_2^i \tag{12}$$

in which i represents the ith cycle of iteration. To update the values of F_1 and F_2, the following iterative equations can be used:

$$F_1^{i+1} = F_1^i + \delta F_1^i = F_1^i + \alpha_1^i \delta H^i + \alpha_2^i \delta V^i \tag{13}$$
$$F_2^{i+1} = F_2^i + \delta F_2^i = F_2^i + \alpha_3^i \delta H^i + \alpha_4^i \delta V^i \tag{14}$$

in which $\alpha^i{}_1$, $\alpha^i{}_2$, $\alpha^i{}_3$, $\alpha^i{}_4$ are correction factors. The iterative process is repeated until the error vector J^iJ (referring to Figure 3) converges to a value lower than the prescribed tolerance limit. By making use of the relationship between elemental nodal-force and incremental-displacement, the stiffness matrix of the cable element can be written as [5]

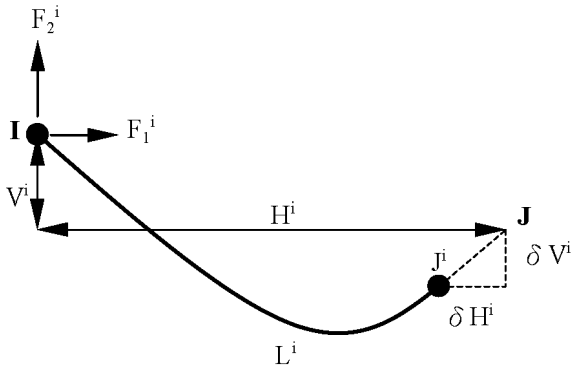

Figure 3. Schematic presentation of error vector J^iJ.

$$[K]=\begin{bmatrix} C & -C \\ -C & C \end{bmatrix} \tag{15}$$

The matrix C is in the following form:

$$[C]_{3\times3}=\begin{bmatrix} -\frac{F_1}{H}m^2-\alpha_1 l^2 & \frac{F_4}{H}lm-\alpha_1 m & -\alpha_2 l \\ & -\frac{F_1}{H}l^2-\alpha_1 m^2 & -\alpha_2 m \\ SYM. & & -\alpha_4 \end{bmatrix} \tag{16}$$

where

$$l=\sin\beta\ ;\ m=\cos\beta \tag{17}$$

and β is the inclination of the local Y_LZ_L-plane with the global YZ-plane.

The end-restraint springs in Figure 1 are used for modeling the tensile restraints provided by a series of transmission towers located beyond either end of the system. In the current study, the stiffness of any end-restraint spring placed along certain direction will be chosen as 1.5 times the stiffness of a single tower, measured in the same direction as that of the end-restraint spring.

2.2 Tower Structures

2.2.1 Formulation for Material Nonlinearity

The component members of each transmission tower in the system will be modeled by using the 3D beam-column elements. To account for the material nonlinearity, the stress-strain relationship of all these elements will be assumed following the relationship as exhibited in an elastic-strain hardening model (referring to Figure 4). In Figure 4, σ_{cy} and σ_{ty} are the yielding stresses corresponding to tensile and compressive deformations respectively and α is called strain-hardening parameter.

Observing the strain distribution along the depth of the beam-column element, as illustrated in Figure 5, one can get the strain ε at a distance η from the centroidal axis of the cross section considered by using the following equation:

$$\varepsilon=\Psi\eta+\varepsilon_0 \tag{18}$$

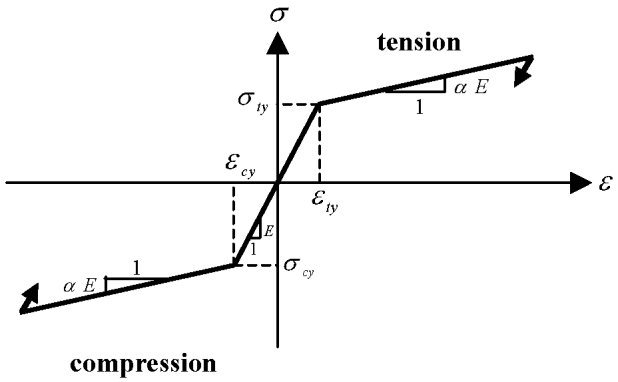

Figure 4. Model of elastic-strain hardening.

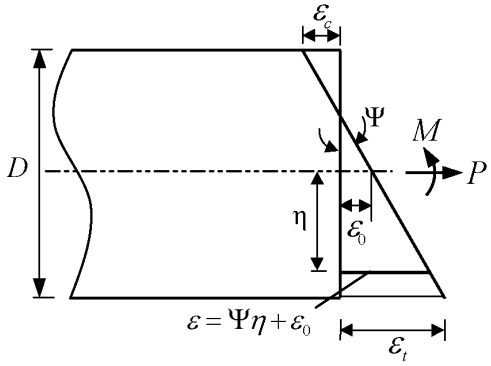

Figure 5. Strain distribution along element depth.

where Ψ is the curvature of the cross section and ε_0 is the strain along centroidal axis. Furthermore, having recognizing that the neutral axis won't be coincident with the centroidal axis due to the existence of internal axial force in the current cases, one can obtain the unyielding depths corresponding to tensile and compressive deformations, denoted as η_{ty} and η_{cy} respectively, by making use of the relations in the following.

$$\eta_{ty}=\frac{1}{\Psi}(\varepsilon_y-\varepsilon_0) \ \le\ \frac{D}{2} \tag{19}$$

$$\eta_{cy}=\frac{1}{\Psi}(-\varepsilon_y-\varepsilon_0) \ \ge\ -\frac{D}{2} \tag{20}$$

Accordingly, the stress at any depth of cross section can be written as

$$\sigma=\begin{cases} \alpha E(\Psi\eta+\varepsilon_0+\varepsilon_y)-E\varepsilon_y & (\eta\le\eta_{cy}) \\ E(\Psi\eta+\varepsilon_0) & (\eta_{cy}\le\eta\le\eta_{ty}) \\ \alpha E(\Psi\eta+\varepsilon_0-\varepsilon_y)+E\varepsilon_y & (\eta\ge\eta_{ty}) \end{cases} \tag{21}$$

in which E is the modulus of elasticity, σ is the normal stress corresponding to ε_0, and ε_y is the yielding strain.

To make the expressions of σ be more concise, the symbol $\langle S\rangle$ is introduced, with the use of the definition given by

$$\langle S\rangle = \begin{cases} S & (0 \le S) \\ 0 & (0 \ge S) \end{cases} \tag{22}$$

Consequently, Eq. (21) can be rewritten as

$$\sigma = E\Big[\Psi\eta + \varepsilon_0 - (1-\alpha)\langle\Psi\eta + \varepsilon_0 - \varepsilon_y\rangle + (1-\alpha)\langle -\Psi\eta - \varepsilon_0 - \varepsilon_y\rangle\Big] \tag{23}$$

Equating the total axial force P with the resultant of the components for axial force, and also equating the total moment M with the resultant of the components for flexural force leads to

$$P = \int_{-D/2}^{D/2}\sigma\ dA = B\int_{-D/2}^{D/2}\sigma\ d\eta = BE\int_{-D/2}^{D/2}\Big[(\Psi\eta + \varepsilon_0) - (1-\alpha)\langle\Psi\eta + \varepsilon_0 - \varepsilon_y\rangle + (1-\alpha)\langle -\Psi\eta - \varepsilon_0 - \varepsilon_y\rangle\Big]\ d\eta \tag{24}$$

$$M = \int_{-D/2}^{D/2}\sigma\eta\ dA = B\int_{-D/2}^{D/2}\sigma\eta\ d\eta = BE\int_{-D/2}^{D/2}\Big[(\Psi\eta + \varepsilon_0) - (1-\alpha)\langle\Psi\eta + \varepsilon_0 - \varepsilon_y\rangle + (1-\alpha)\langle -\Psi\eta - \varepsilon_0 - \varepsilon_y\rangle\Big]\ \eta d\eta \tag{25}$$

in which B is the width of cross section.

With further calculations, the above two equations can be expressed in more concise forms:

$$P = EA\left\{\varepsilon_0 + (1-\alpha)\frac{D}{8\Psi}\left[\left\langle\Psi - \Psi_y\left(1+\frac{\varepsilon_0}{\varepsilon_y}\right)\right\rangle^2 - \left\langle\Psi - \Psi_y\left(1-\frac{\varepsilon_0}{\varepsilon_y}\right)\right\rangle^2\right]\right\} \tag{26}$$

$$M = EI\Psi\left\{1 - \frac{(1-\alpha)}{2}\left\langle 1 - \frac{\Psi_y}{\Psi}\left(1+\frac{\varepsilon_0}{\varepsilon_y}\right)\right\rangle^2\left[1 - \frac{\Psi_y}{2\Psi}\left(1+\frac{\varepsilon_0}{\varepsilon_y}\right)\right] - \frac{(1-\alpha)}{2}\left\langle 1 - \frac{\Psi_y}{\Psi}\left(1-\frac{\varepsilon_0}{\varepsilon_y}\right)\right\rangle^2\left[1 + \frac{\Psi_y}{2\Psi}\left(1-\frac{\varepsilon_0}{\varepsilon_y}\right)\right]\right\} \tag{27}$$

Introducing the dimensionless parameters p, m, ψ and $\bar{\varepsilon}_0$ into Eqs. (26) and (27) leads to

$$p = \bar{\varepsilon}_0 + \frac{(1-\alpha)}{4}\Big[\langle\psi - 1 - \bar{\varepsilon}_0\rangle^2 - \langle\psi - 1 + \bar{\varepsilon}_0\rangle^2\Big] \tag{28}$$

$$m = \psi - \frac{(1-\alpha)}{4\varphi^2}\Big[\langle\psi - 1 - \bar{\varepsilon}_0\rangle^2(2\psi + 1 + \bar{\varepsilon}_0) - \langle\psi - 1 + \bar{\varepsilon}_0\rangle^2(2\psi + 1 - \bar{\varepsilon}_0)\Big] \tag{29}$$

in which

$$p = \frac{p}{p_y}\ ;\ m = \frac{M}{M_y}\ ;\ \psi = \frac{\Psi}{\Psi_y}\ ;\ \bar{\varepsilon}_0 = \frac{\varepsilon_0}{\varepsilon_y} \tag{30}$$

The subscript y in Eq. (30) is used to denote the state of yielding. Eliminating the parameter $\bar{\varepsilon}_0$ by solving Eq. (28) and Eq. (29) simultaneously gives p–m–ψ relationships in various conditions:

(i) The tensile and compressive zones are all in initial elastic range, namely in the case of $\psi \le \psi_{et}$ and $\psi \le \psi_{ec}$:

$$m = \psi \tag{31}$$

(ii) The compressive zone is all in initial elastic range whereas a portion of the tensile zone has been deformed into the subsequent strain-hardening range, namely in the case of $\psi_{et} \le \psi_{ec}$ and $\psi_{et} \le \psi \le \psi_{tc}$:

$$m = \psi - \frac{(1-\alpha)}{4\psi^2}(\psi - 1 + \bar{\varepsilon}_0)^2(2\psi + 1 - \bar{\varepsilon}_0) \tag{32}$$

where

$$\bar{\varepsilon}_0 = \frac{1 - \alpha + \psi + \alpha\psi - 2\sqrt{\psi[(1-\alpha)(1-p) + \alpha\psi]}}{1-\alpha} \tag{33}$$

(iii) The tensile zone is all in initial elastic range whereas a portion of the compressive zone has been deformed into the subsequent strain-hardening range, namely in the case of $\psi_{ec} \le \psi_{et}$ and $\psi_{ec} \le \psi \le \psi_{ct}$:

$$m = \psi - \frac{(1-\alpha)}{4\psi^2}(\psi - 1 - \bar{\varepsilon}_0)^2(2\psi + 1 + \bar{\varepsilon}_0) \tag{34}$$

where

$$\bar{\varepsilon}_0 = \frac{-1+\alpha-\psi-\alpha\psi+2\sqrt{\psi[(1-\alpha)(1-p)+\alpha\psi]}}{1-\alpha} \quad (35)$$

(iv) Both a portion of tensile and a portion of compressive zones have been deformed into the strain-hardening range, namely in the case of $\psi_{tc} \le \psi$ or $\psi_{ct} \le \psi$:

$$m = \psi - \frac{(1-\alpha)}{4\psi^2}\Big[(\psi-1-\bar{\varepsilon}_0)^2(2\psi+1+\bar{\varepsilon}_0) + (\psi-1+\bar{\varepsilon}_0)^2(2\psi+1-\bar{\varepsilon}_0)\Big] \quad (36)$$

where

$$\bar{\varepsilon}_0 = \frac{p\psi}{1-\alpha+\alpha\psi} \quad (37)$$

In the above discussion, each of the boundary curvatures ψ_{et}, ψ_{ec}, ψ_{tc} and ψ_{ct} will be associated with a specific stress distribution as described in the following.

(a) When the whole compressive zone is still in elastic range but the tensile zone has been just beginning to yield, the curvature of the cross section, denoted as ψ_{et}, would be

$$\psi_{et} = 1 - p \quad (38)$$

(b) When the whole tensile zone is still in elastic range but the compressive zone has been just beginning to yield, the curvature of the cross section, denoted as ψ_{ec}, would be

$$\psi_{ec} = 1 + p \quad (39)$$

(c) When a portion of the tensile zone has come to yield already but the compressive zone is at the moment just beginning to yield, the curvature of the cross section, denoted as ψ_{tc}, would be

$$\psi_{tc} = \frac{2(1-\alpha)}{(1-p)-2\alpha+\sqrt{(1-p)^2+4p\alpha}} \quad (40)$$

(d) When a portion of the compressive zone has come to yield already but the tensile zone is at the moment just beginning to yield, the curvature of the cross section, denoted as ψ_{ct}, would be

$$\psi_{ct} = \frac{2(1-\alpha)}{(1+p)-2\alpha+\sqrt{(1+p)^2-4p\alpha}} \quad (41)$$

Figure 6 shows the $m-\psi$ relationships under various values of p with $\alpha = 0$. It can be seen that the variation of the slope for the curves in the figure consists of three main stages: (1) a considerably large value of slope kept constant until the outer fiber of the section is on the edge of yielding (2) a medium value of slope varied gradually until the whole section has come to yield (3) a value of slope kept being zero lastingly. Since the slope of any $m-\psi$ curve is also the flexural rigidity of the cross section, EI, corresponding to certain axial force, a modified flexural rigidity, $(EI)_{ave}$, obtained by taking the average of the sum of the rigidities corresponding to five equally spaced sections, will be adopted as the flexural rigidity of a single beam-column element.

2.2.2 Formulation for Geometric Nonlinearity

In taking the effect of geometric nonlinearity into account, a Cartesian coordinate system composed of x-, y- and z- axes as illustrated in Figure 7 is adopted as the local coordinate system of the beam-column element. The longitudinal direction of the element will be as-

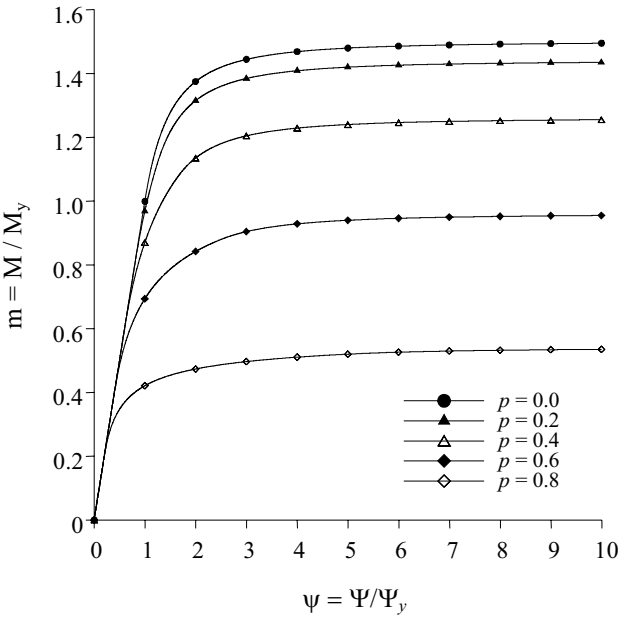

Figure 6. $m-\psi$ relationship ($\alpha = 0$).

sumed to be coincident with the x-axis, and the two principal axes perpendicular each other over the cross section would be set in y- and z-directions respectively. In Figure 7, $u_{1,}$ u_2 and u_3 represent the translational displacements at the left end of the element in x-, y- and z-directions respectively; $u_{7,}$ u_8 and u_9 represent the translational displacements at the right end of the element in x-, y- and z-directions respectively; $u_{4,}$ u_5 and u_6 represent the rotational displacements at the left end of the element around x-, y- and z-axes respectively; $u_{10,}$ u_{12} and u_6 represent the rotational displacements at the right end of the element around x-, y- and z-axes respectively. Besides, the nodal force corresponding to the nodal displacement u_i (i = 1, 2, ….., 12) will be denoted by using the symbol $F_{i.}$ The stiffness matrix of the element in Figure 7 would be in the form as written in the following.

$$[k]=\begin{bmatrix} k(1,1) & k(1,2) & \cdots & \cdots & k(1,12) \\ k(2,1) & k(2,2) & \cdots & \cdots & k(2,12) \\ \cdots & \cdots & \cdots & \cdots & \cdots \\ \cdots & \cdots & \cdots & \cdots & \cdots \\ k(12,1) & k(12,2) & \cdots & \cdots & k(12,12) \end{bmatrix} \tag{42}$$

With the application of the beam-column approach, the stiffness coefficient k(i, j) (i, j = 1, 2, …, 12) which includes the effect of both material and geometric nonlinearities can be obtained as follows:

$$k(1,1)=k(7,7)=-k(1,7)=\frac{EA}{L}R_t \tag{43}$$

$$k(2,2)=k(8,8)=-k(2,8)=\frac{(EI_z)_{ave}}{L^3}S_{1z} \tag{44}$$

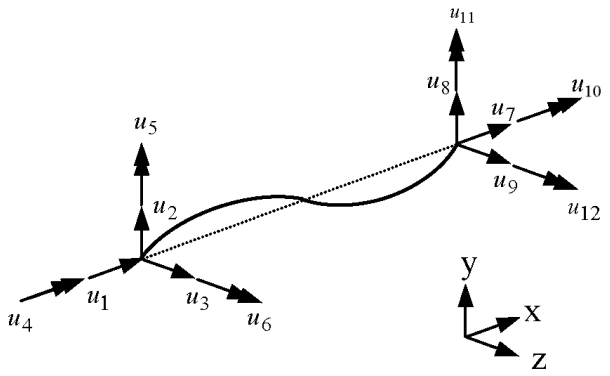

Figure 7. Nodal displacement of 3-D beam-column element.

$$k(2,6)=k(2,12)=-k(6,8)=-k(8,12) =-\frac{(EI_z)_{ave}}{L^2}S_{2z} \tag{45}$$

$$k(3,5)=k(3,11)=-k(5,9)=-k(9,11) =-\frac{(EI_y)_{ave}}{L^2}S_{2y} \tag{46}$$

$$k(4,4)=k(10,10)=-k(4,10)=\frac{GJ}{L} \tag{47}$$

$$k(5,5)=k(11,11)=\frac{(EI_y)_{ave}}{L}S_{3y} \tag{48}$$

$$k(6,6)=k(12,12)=\frac{(EI_z)_{ave}}{L}S_{3z} \tag{49}$$

$$k(5,11)=\frac{(EI_y)_{ave}}{L}S_{4y} \tag{50}$$

$$k(6,12)=\frac{(EI_z)_{ave}}{L}S_{4z} \tag{51}$$

where E is the modulus of elasticity; A and L are the cross-sectional area and length of the beam-column element respectively; I_y and I_z are the moments of inertia corresponding to y- and z-axes respectively; J is the polar moment of inertia; G is the shear modulus of elasticity; R_t is the axial stiffness coefficient used for taking the bowing effect, that is the effect of the axial deformation caused by flexural force, into account. The stability functions S_{jy} and S_{jz} (j = 1, 2, 3, 4) in the above equations, used for taking the effect of the interaction between axial and flexural forces into consideration, are derived to be:

(i) When the internal axial force is in compression ($F_1 = -F_7 > 0$):

$$S_{1y}=\frac{\hat{\phi}_y^3\sin\hat{\phi}_y}{(2-2\cos\hat{\phi}_y-\hat{\phi}_y\sin\hat{\phi}_y)} \tag{52}$$

$$S_{2y}=\frac{\hat{\phi}_y^3(1-\cos\hat{\phi}_y)}{(2-2\cos\hat{\phi}_y-\hat{\phi}_y\sin\hat{\phi}_y)} \tag{53}$$

$$S_{3y}=\frac{\hat{\phi}_y(\sin\hat{\phi}_y-\hat{\phi}_y\cos\hat{\phi}_y)}{(2-2\cos\hat{\phi}_y-\hat{\phi}_y\sin\hat{\phi}_y)} \tag{54}$$

$$S_{4y}=\frac{\hat{\phi}_y(\hat{\phi}_y-\hat{\phi}_y\sin\hat{\phi}_y)}{(2-2\cos\hat{\phi}_y-\hat{\phi}_y\sin\hat{\phi}_y)} \tag{55}$$

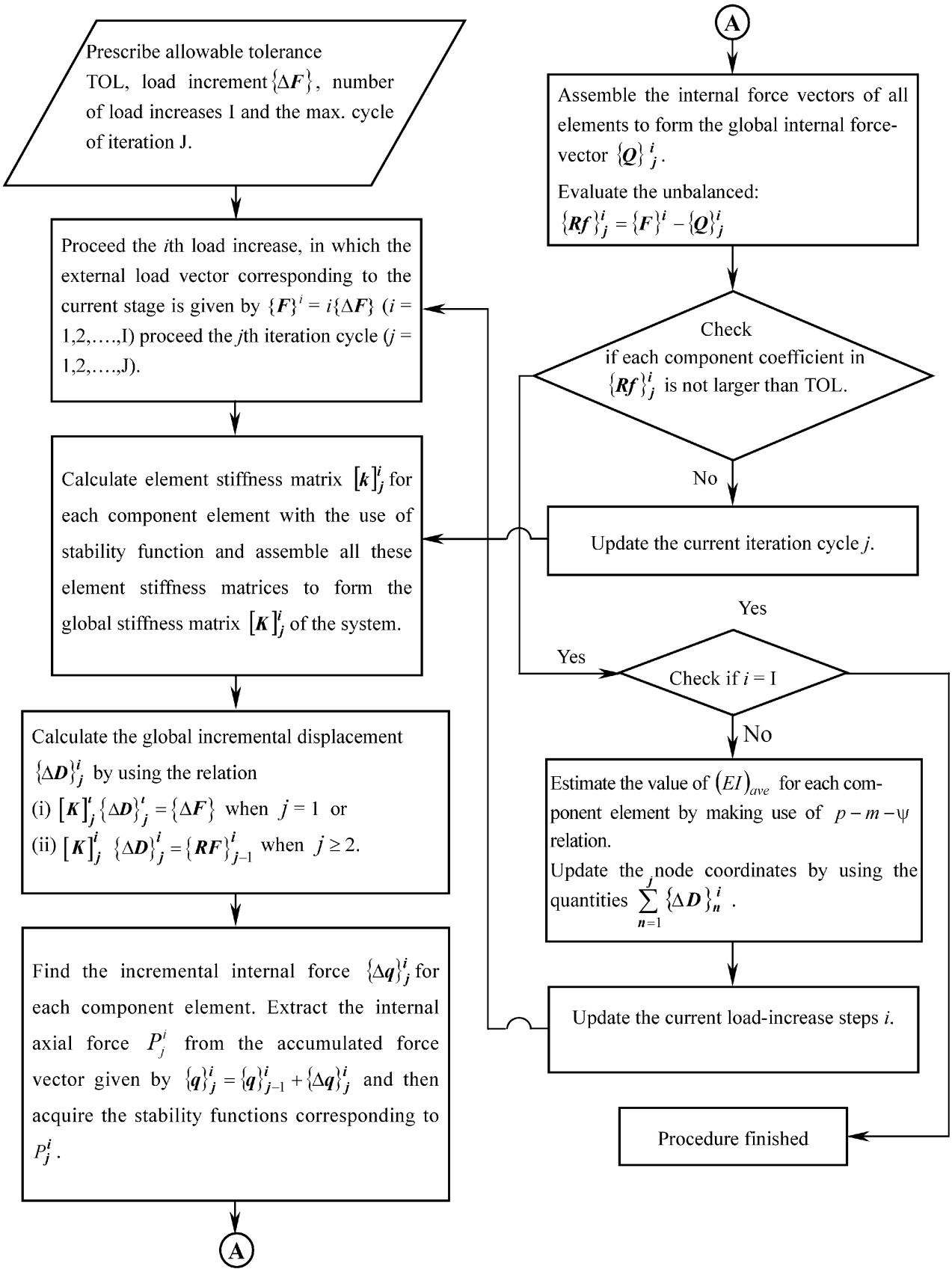

Figure 8. Flowchart of acquiring the nonlinear stiffness matrix.

in which

$$\hat{\phi}_y = \sqrt{\frac{PL^2}{EI_y}} \tag{56}$$

(ii) When the internal axial force is in tension ($F_1 = -F_7 < 0$):

$$S_{1y} = \frac{\hat{\phi}_y^3 \sinh\hat{\phi}_y}{(2-2\cosh\hat{\phi}_y + \hat{\phi}_y \sinh\hat{\phi}_y)} \tag{57}$$

$$S_{2y} = \frac{\hat{\phi}_y^3 (\cosh\hat{\phi}_y - 1)}{(2-2\cosh\hat{\phi}_y + \hat{\phi}_y \sinh\hat{\phi}_y)} \tag{58}$$

$$S_{3y} = \frac{\hat{\phi}_y (\hat{\phi}_y \cosh\hat{\phi}_y - \sinh\hat{\phi}_y)}{(2-2\cosh\hat{\phi}_y + \hat{\phi}_y \sinh\hat{\phi}_y)} \tag{59}$$

$$S_{4y} = \frac{\hat{\phi}_y (\hat{\phi}_y \sinh\hat{\phi}_y - \hat{\phi}_y)}{(2-2\cosh\hat{\phi}_y + \hat{\phi}_y \sinh\hat{\phi}_y)} \tag{60}$$

Replacing I_y in Eqs. (52)-(55) & (57)-(60) with I_z leads to the shifting of the quantities on the left-hand side of these equations from S_{jy} (j = 1,2,3,4) to S_{jz}. In undertaking the seismic time-history analysis, Newton-Raphson method will be adopted as the iterative scheme for modifying the stiffness coefficients in Eqs. (43)–(51) repeatedly at each time step until the attainment of convergence. The procedure for acquiring the nonlinear elemental stiffness matrix is illustrated by the flowchart shown in Figure 8.

3. Numerical Examples

The acceleration of Ji-Ji earthquake, recorded at TCU084 station in Taichung, Taiwan, with the peak value of 1.00834 g is taken as the ground excitation acting on the structural system. Figure 9 shows the Fourier spectrum for the acceleration. As indicated in Figure 1, each of the structural systems investigated in the following will include three tower structures, in which the towers M and N are located at two ends, and the tower O is located in the middle of the system. The distance between adjacent towers is chosen to be 350 meters. The electrical wires suspending between two towers is prescribed by a length of 360 meters and will be modeled by using four cable elements aforementioned. Figure 10 shows the structural pattern of each tower in the system. Table 1 specifies the cross-sectional properties of tower members and wires. For simplification of calculations, all the investigations regarding to the internal-force variation of structural elements will be mainly focused upon the four leg members, named Leg A, Leg B, Leg C and Leg D respectively (referring to Figure 11), at the bottom of tower N. Further-

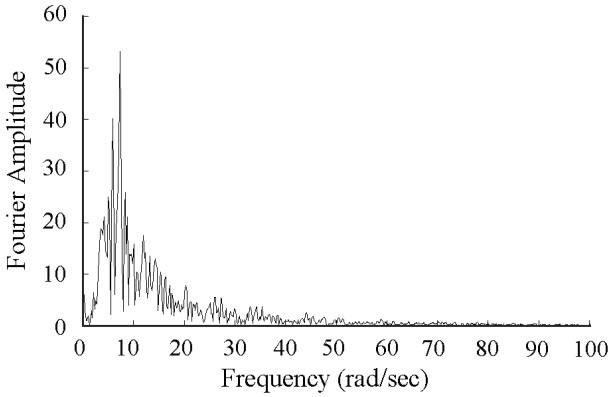

Figure 9. Fourier spectrum of acceleration.

Table 1. Sectional properties of tower members & electric wires

Sectional Parameter	Region I		Region II		Region III		Conduct Wire	Ground Wire
	Leg Member	Diagonal Member	Leg Member	Diagonal Member	Leg Member	Diagonal Member		
A (m^2)	4.47×10^{-3}	2.75×10^{-3}	4.30×10^{-3}	2.75×10^{-3}	3.50×10^{-3}	2.49×10^{-3}	4.69×10^{-4}	1.59×10^{-4}
E (N/m^2)	2.00×10^{11}	2.00×10^{11}	2.00×10^{11}	2.00×10^{11}	2.00×10^{11}	2.00×10^{11}	8.90×10^{4}	1.05×10^{5}
G (N/m^2)	7.69×10^{10}	7.69×10^{10}	7.69×10^{10}	7.69×10^{10}	7.69×10^{10}	7.69×10^{10}	--	--
P (kg/m^3)	7,850	7,850	7,850	7,850	7,850	7,850	--	--
$\overline{\rho}$ (kg/m)	--	--	--	--	--	--	1.628	1.062
I_y or I_z (m^4)	1.82×10^{-6}	6.29×10^{-7}	1.54×10^{-6}	6.29×10^{-7}	1.02×10^{-6}	5.16×10^{-7}	--	--
J (m^4)	3.63×10^{-6}	1.26×10^{-6}	3.09×10^{-6}	1.26×10^{-6}	2.04×10^{-6}	1.03×10^{-6}	--	--
P_y (N/m^2)	1,116,500	686,500	1,076,000	686,500	874,750	622,250	--	--
M_{py} or M_{pz} (N-m)	18,653.40	8,993.54	17,647.71	8,993.54	3,233.97	7,760.99	--	--

more, in order to investigate the load effects due to the acting direction of earthquake, the term "input angle of seismic force", denoted by using the symbol λ, is defined as the angle of seismic force, measured counterclockwise from the positive direction of X-axis, as illustrated in Figure 11. In actual calculation, λ will range from zero to 180 degrees with the angle increment of 15 degrees.

3.1 Configurations of Transmission Towers

In the following numerical examples, seismic analyses will be performed with respect to a group of towers exhibited in various configurations. To describe the position of tower N relative to that of towers M and O in a tower group, the parameters of θ and ϕ, called horizontal and vertical angles respectively, will be introduced in this study. Figures 12 and 13 show the illustration of these parameters.

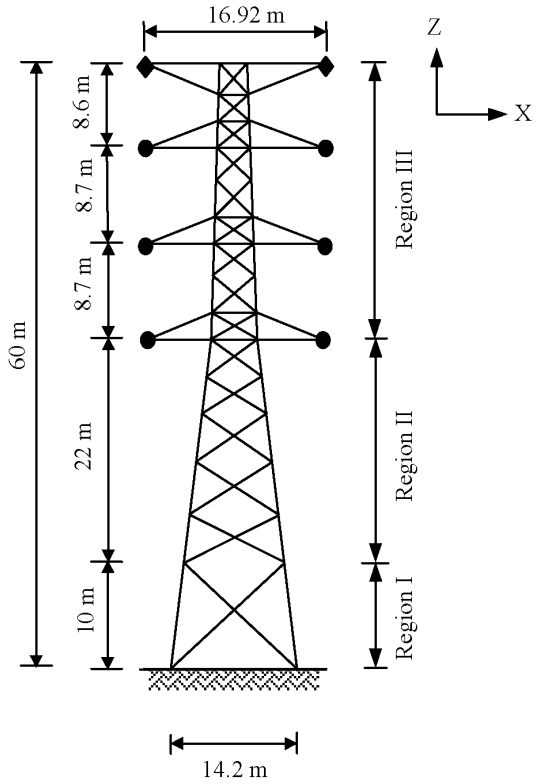

Figure 10. Structural pattern of transmission tower.

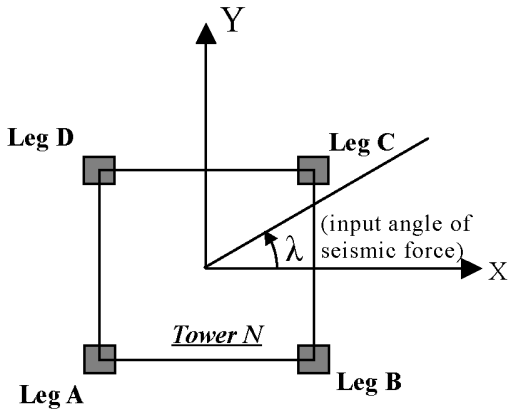

Figure 11. Legs at tower bottom and input angle of seismic force.

3.2 Failure Index

The failure of the transmission tower can be triggered by the fracture of any component main-member in the structure. This member fracture is usually not caused by the action of single type of internal force, but by the combined action resulting from various kinds of internal forces including axial, flexural and shear forces. According to the theory proposed by Chen and Atsuta, the beam-column element exhibiting an elastic-perfectly plastic behavior (that is the case of $\alpha = 0$) and having a cross section in rectangle will reach its ultimate strength if the interaction-strength equations expressed in the following are satisfied [8].

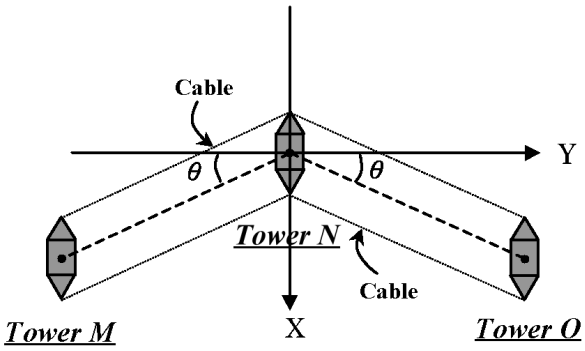

Figure 12. Description of horizontal angle θ.

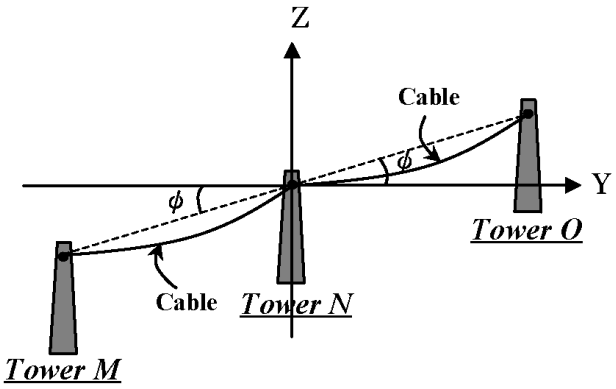

Figure 13. Description of vertical angle ϕ.

$$\text{(i)}\quad m_y \geq \frac{2}{3}(1-p) \text{ and } m_z \leq \frac{2}{3}(1-p): \qquad p^2 + m_y + \frac{3}{4}m_z^2 \leq 1 \tag{61}$$

$$\text{(ii)}\quad m_y \leq \frac{2}{3}(1-p) \text{ and } m_z \geq \frac{2}{3}(1-p): \qquad p^2 + \frac{3}{4}m_y^2 + m_z \leq 1 \tag{62}$$

$$\text{(iii)}\quad m_y \geq \frac{2}{3}(1-p) \text{ and } m_z \geq \frac{2}{3}(1-p): \qquad p + \frac{9}{4}\left[1 - \frac{m_y}{2(1-p)}\right]\left[1 - \frac{m_z}{2(1-p)}\right] \leq 1 \tag{63}$$

In Eqs. (61)-(63), the dimensionless parameters of p, m_y and m_z are defined, respectively, as

$$p = \frac{P}{P_y} \;;\; m_y = \frac{M_y}{M_{py}} \;;\; m_z = \frac{M_z}{M_{pz}} \tag{64}$$

in which P is the axial force acting on the cross section; M_y and M_z are the applied moments around the principal y- and z-axes respectively; P_y is the axial yielding strength; M_{py} and M_{pz} are the ultimate plastic moments around the principal y- and z-axes respectively.

Since being a useful index in the judgment of member fracture, the quantities on the left-hand side of Eqs. (61)-(63) will be given the name "failure index", which is denoted by using the symbol Λ. Accordingly, the curved surface indicated in Figure 14 will be the enveloped surface of fracture, and each point on the surface would correspond to an identical value of Λ = 1. In addition, the shaded area in the figure would represent the interaction plane associated with the loading conditions in which the axial ratio p has a fixed value of 0.5. In undertaking the seismic analysis for the cases described in numerical examples, it is assumed that the global failure of a transmission tower arises whenever the failure index corresponding to any component member of this tower is found equal or greater than unity.

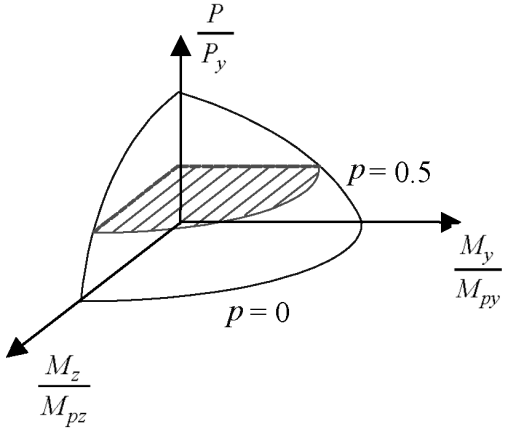

Figure 14. Failure surface of beam-column elements.

4. Results and Discussion

To inspect the effect of wire action on the dynamic behavior of transmission towers, the variation of Λ for Legs C and D in the cases of the structures being either connected or not connected with electrical wires (Both wire action and wire mass are neglected in the latter case) is shown in Figure 15. It is observed that the difference between the curves corresponding to these two cases is considerably significant.

4.1 Variation of Λ due to θ

In the condition of ϕ = 0°, the bases of towers M, N and O would lie on the XY-plane and be symmetric with respect to the X-axis (referring to Figure 13), so the investigation of Λ will be focused upon Legs C and D only. It is observed in Figures 16 and 17 that with a few exceptions only, the larger the value of θ is the larger the failure index will usually be. In addition, since the peak value of Λ for Leg D is found greater than unity, the fracture of this member can then be expected according to the interpretation of the interaction equations in Sec. *3.2.*

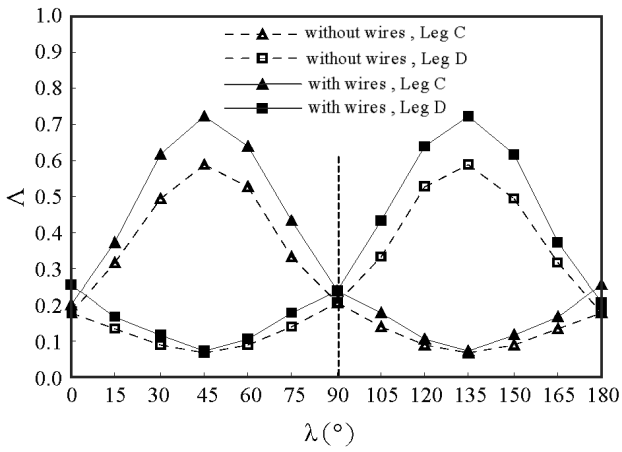

Figure 15. Effect on failure index caused by cable action (θ = ϕ = 0°).

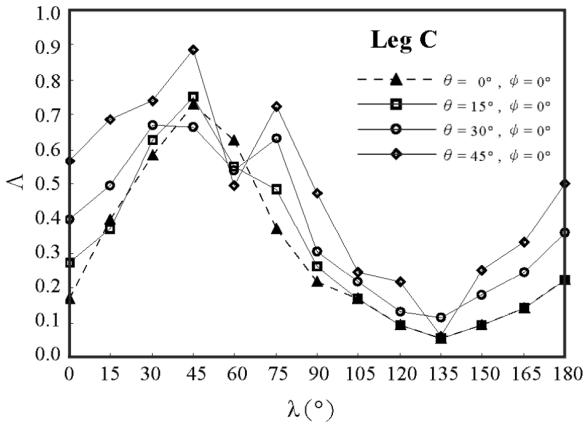

Figure 16. Failure index of Leg C with $\phi = 0°$ under varied θ.

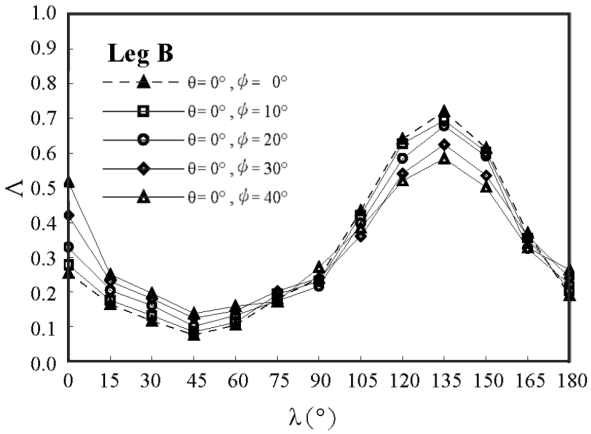

Figure 18. Failure index of Leg B with $\theta = 0°$ under varied ϕ.

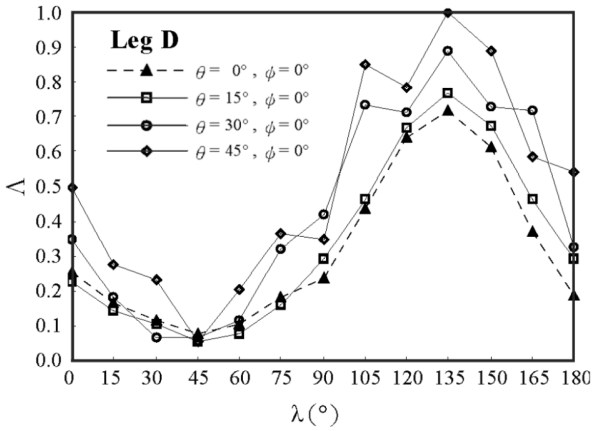

Figure 17. Failure index of Leg D with $\phi = 0°$ under varied θ.

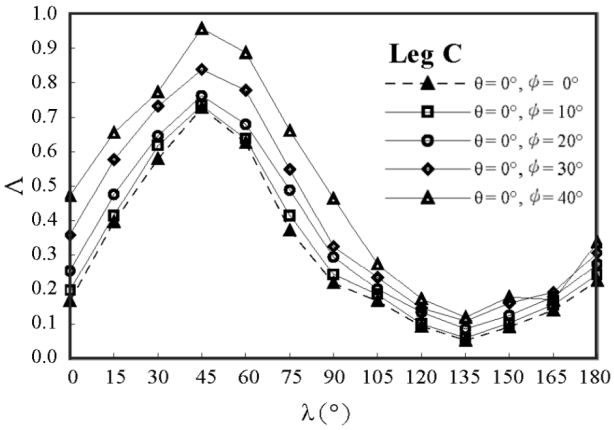

Figure 19. Failure index of Leg C with $\theta = 0°$ under varied ϕ.

4.2 Variation of Λ due to ϕ

In the condition of $\theta = 0°$, the failure index corresponding to $\lambda = \lambda^*$ for Legs A and C would be equal to that corresponding to $\lambda = \pi - \lambda^*$ for Legs B and D respectively (referring to Figures 11-13), so the investigation of Λ will be focused upon Legs B and C only. It is observed in Figures 18 and 19 that no matter what value the parameter ϕ is, the peak values of failure index on each curve would occur at $\lambda = 135°$ and $45°$ for Legs B and C respectively. This implies that under certain prescribed value of ϕ, the peak failure index would occur at the time when the seismic force is parallel to the diagonal, which passes through Leg B or C, of the base of tower N. In addition, it is noticed that the peak failure index corresponding to $\phi = 0°$ for Leg B would be larger than those corresponding to other values of ϕ; this specific value of ϕ will be shifted from 0° to 40° for Leg C, however.

4.3 Variation of Λ under Various Combinations of ϕ and θ

To investigate the safety of tower members under all kinds of configurations of transmission towers, Figures 20-23 are presented for this purpose. It is observed in the first two figures that under a varied θ and a prescribed ϕ, the larger the value of ϕ is, the larger the peak failure index and the higher the probability of member fracture will usually be. Similar phenomenon will also be observed under a varied ϕ and a prescribed θ, as indicated in Figures 23 and 24. To get a better understanding to the variation tendency of the curves in Figures 20-23, a plot of average failure index, Λ_{ave}, versus input angle of seismic force, λ, is presented in Figures 24 and 25, in which the ordinate coordinate of any point on a curve is obtained by taking the average of the failure-index values corresponding to an identi-

cal λ. Except for a few cases, the phenomenon observed in both figures matches fairly well with that observed in Figures 20-23.

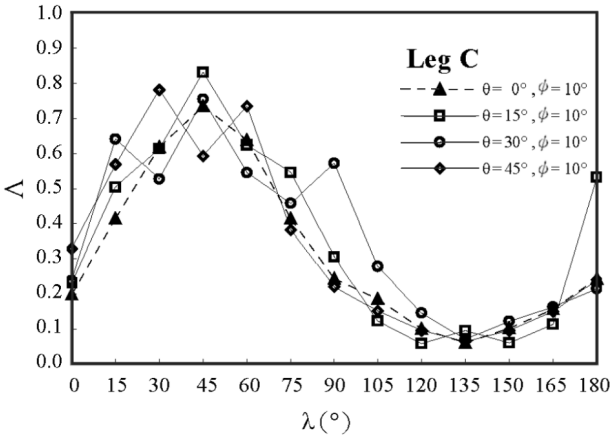

Figure 20. Failure index of Leg C with ϕ = 10° under varied θ.

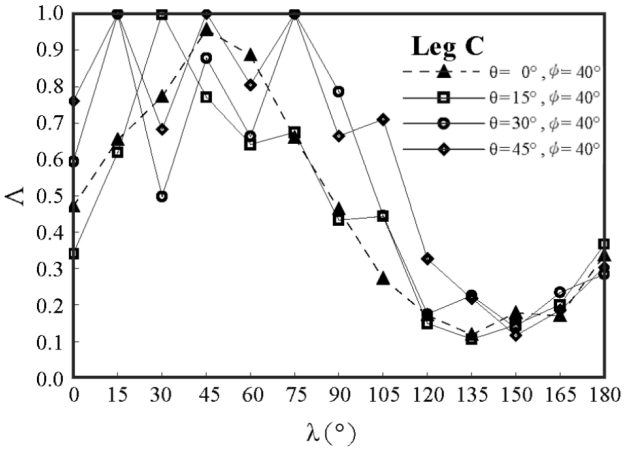

Figure 21. Failure index of Leg C with ϕ = 40° under varied θ.

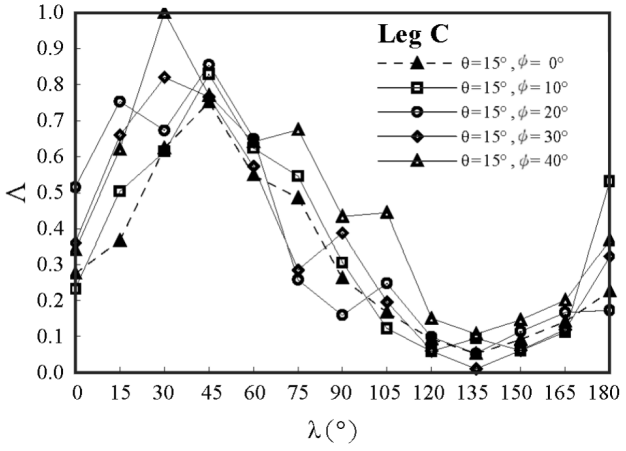

Figure 22. Failure index of Leg C with θ = 15° under varied ϕ.

5. Conclusions

Having undertaken the seismic analysis in consider-

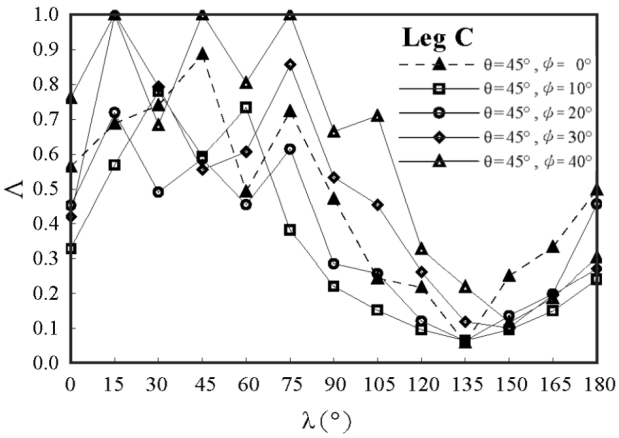

Figure 23. Failure index of Leg C with θ = 45° under varied ϕ.

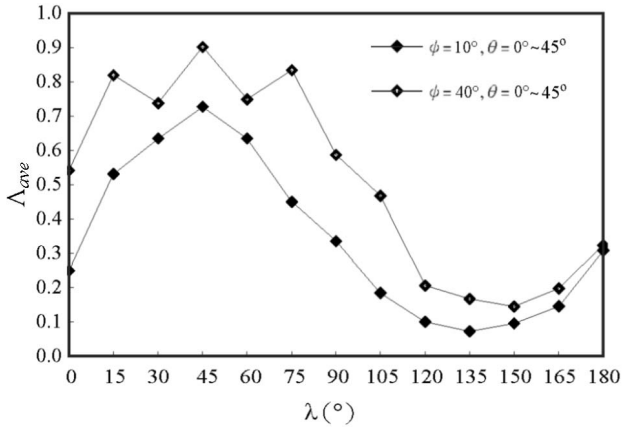

Figure 24. Average failure index of Leg C with ϕ = 10° and 40°.

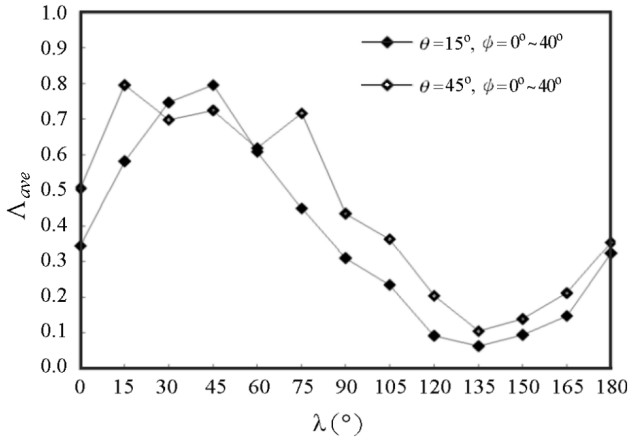

Figure 25. Average failure index of Leg C with θ = 15° and 45°.

ation of both material and geometric nonlinearities, with respect to the structural system modeled by using beam-column elements, cable elements and end-restraint elements, one may recognize that ignoring the wire-action effect on the dynamic behavior of transmission towers may cause significant errors in the results of member forces.

In the condition of $\phi = 0°$, the larger the value of θ is the larger the failure index will usually be. On the other hand, in the condition of $\theta = 0°$, the peak failure index would occur at the time when the seismic force is parallel to the diagonal, which passes through the leg member considered, of the tower base.

Under a varied θ and a prescribed ϕ, the larger the value of ϕ is, the larger the peak failure index and the higher the probability of member fracture will usually be. Similar phenomenon will also be observed under a varied ϕ and a prescribed θ.

Acknowledgment

The work has been supported by research grants made by the National Science Council (Taiwan, Republic of China) under grant No. NSC 93-2211-E-032-008.

References

[1] Albermani, F. G. A. and Kitipornchai, S., "Nonlinear Finite Element Analysis of Latticed Transmission Towers," *Engineering Structure*, Vol. 15, pp. 259–269 (1993).

[2] Knight, G. M. S. and Santhakumar A. R., "Joint Effects on Behavior of Transmission Towers," *Journal of Structural Engineering*, Vol. 119, pp. 698–712 (1993).

[3] Kitipornchai, S., AlBermani, F. G. A. and Peyrot A. H., "Effect of Bolt Slippage on The Ultimate Strength of Latticed Structures," *Journal of Structural Engineering*, Vol. 120, pp. 2281–2287 (1994).

[4] Albermani, F. G. A. and Kitipornchai S., "Numerical Simulation of Structural Behaviour of Transmission Towers," *Thin-Walled Structures*, Vol. 41, pp. 167–177 (2003).

[5] Jayaraman, H. B. and Knudson W. C., "A Curved Element for the Analysis of Cable Structure," *Computers and Structures*, Vol. 14, pp. 325–333 (1981).

[6] O'Brien, T., "General Solution of Suspended Cable Problems," *Journal of Structural Division*, Vol. 93, pp. 1–26 (1967).

[7] Peyrot, A. H. and Goulois A. M., "Analysis of Flexible transmission lines," *Journal of Structural Division*, Vol. 104, pp. 763–779 (1978).

[8] Chen, W. F. and Atsuta, T., *Theory of Beam-Columns-Space Behavior and Design Vol. 2*, McGraw-Hill, New York, U.S.A. (1977).

Manuscript Received: Aug. 19, 2004
Accepted: Nov. 5, 2004